

# Langmuir–Blodgett Films of Charge-Transfer Complexes between an Amphiphilic Monopyrrolo-TTF and TCNQ Derivatives

Tomoyuki Akutagawa,<sup>\*,†,‡</sup> Masanori Uchigata,<sup>§</sup> Tatsuo Hasegawa,<sup>†</sup> Takayoshi Nakamura,<sup>\*,†,‡</sup> Kent A. Nielsen,<sup>||</sup> Jan O. Jeppesen,<sup>||</sup> Thomas Brimert,<sup>||</sup> and Jan Becher<sup>||</sup>

Research Institute for Electronic Science, Hokkaido University, Sapporo 060-0812, Japan, Graduate School of Science, Hokkaido University, Sapporo 060-0810, Japan, CREST, Japan Science and Technology Corporation (JST), Kawaguchi 332-0012, Japan, and University of Southern Denmark, Campusvej 55, DK-5230 Odense M, Denmark

Received: August 7, 2003; In Final Form: October 7, 2003

Electrically active Langmuir–Blodgett (LB) films based on charge-transfer (CT) complexes between an amphiphilic monopyrrolo-tetrathiafulvalene (MP-TTF) electron donor and different derivatives of the electron acceptor 7,7,8,8-tetracyano-*p*-quinodimethane (TCNQ), namely, 2,5-difluoro-TCNQ, fluoro-TCNQ, TCNQ, decyl-TCNQ, 2,5-dimethyl-TCNQ, and 2-methoxy-5-ethoxy-TCNQ, have been fabricated and investigated systematically. The electronic ground state of the CT complex, (MP-TTF<sup>+δ</sup>)(TCNQs<sup>-δ</sup>), in the LB films varied from ionic ( $\delta = 1$ ) to neutral ( $\delta \sim 0$ ) depending on the electron affinity of the TCNQ derivative used. CT excitation energies of the LB films were correlated against the difference between the redox potentials of the MP-TTF and TCNQ derivatives, exhibiting agreement with a neutral–ionic (N–I) phase diagram proposed for mixed-stack CT complexes. Of the six kinds of LB films, the (MP-TTF<sup>+0.3</sup>)(decyl-TCNQ<sup>-0.3</sup>) and (MP-TTF<sup>+0.6</sup>)(TCNQ<sup>-0.6</sup>) complexes were located closest to the N–I phase boundary. In all of the LB films, the CT transition moment was found to be parallel to the substrate surface based on information from polarized UV–vis–NIR, IR transmission, and reflection–absorption spectra. After being transferred onto a mica surface by a single withdrawal, the surface morphologies of the films were found to be uniform or exhibited spongelike domain structures of thickness about 1.8 nm.

## Introduction

Molecular assemblies held together by charge-transfer (CT) interactions exhibit peculiar electrical,<sup>1</sup> magnetic,<sup>2</sup> and optical properties,<sup>3</sup> in which the number of conduction carriers, magnetic spin, and optical excitation energy are tunable depending on the magnitude of the intermolecular CT interactions between the electron donor (D) and the electron acceptor (A) molecules. The electronic structure of an open-shell (D<sup>+δ</sup>)(A<sup>-δ</sup>) complex, where  $\delta$  is the degree of CT from D to A, is principally determined by the frontier orbitals of the D and A molecules.<sup>1a</sup> The difference between the energy level of the HOMO and the energy of the vacuum level corresponds to the ionization potential ( $I_p$ ) of D, whereas the energy difference between the LUMO and vacuum levels corresponds to the electron affinity ( $E_a$ ) of A. The magnitude of  $\delta$  within the (D<sup>+δ</sup>)(A<sup>-δ</sup>) complex depends on the relative energy difference between  $E_a$  of A and  $I_p$  of D. The neutral electronic ground state of  $\delta \sim 0$  is obtained under condition where  $E_a > I_p$ , whereas the completely ionic state where  $\delta = 1$  is observed when  $E_a < I_p$ . Electrical conduction is largely influenced by the electronic structure of the (D<sup>+δ</sup>)(A<sup>-δ</sup>) complex. The neutral CT complex (D<sup>0</sup>)(A<sup>0</sup>) is an insulator due to a small number of conduction carriers, whereas the completely ionic CT complex (D<sup>+1</sup>)(A<sup>-1</sup>) is also an insulator due to large on-site Coulomb repulsive energies.<sup>2</sup>

Metallic electrical conduction is usually obtained for  $\delta$  values in the range of 0.5–1. For example, the molecular metal composed of tetrathiafulvalene (TTF) and 7,7,8,8-tetracyano-*p*-quinodimethane (TCNQ) exhibits an electronic ground state of (TTF<sup>+0.59</sup>)(TCNQ<sup>-0.59</sup>).<sup>1a,4</sup> Therefore, control of the degree of CT in (D<sup>+δ</sup>)(A<sup>-δ</sup>) complexes is important in order to control the electrical properties of CT complexes. Another important factor for determining the electronic properties of a (D<sup>+δ</sup>)(A<sup>-δ</sup>) complex is the molecular orientation within the molecular assembly.<sup>1a</sup> Typically, D and A molecules exhibit planar conjugated  $\pi$  planes, which tend to form one-dimensional  $\pi$ – $\pi$  stacking structures. In (D<sup>+δ</sup>)(A<sup>-δ</sup>) complexes, two kinds of  $\pi$ –stacking modes are typically observed. The first one is the segregated-stack structure, in which the D (A) molecules stack themselves in a  $\sim D \sim D \sim D \sim (\sim A \sim A \sim A \sim)$   $\pi$ –stacking sequence.<sup>1</sup> Molecular metals such as the (TTF)(TCNQ) CT complex form uniform segregated-stack structures,<sup>4</sup> which are stabilized by the formation of a  $\pi$  band. The second one is the mixed-stack structure, in which D and A molecules are stacked alternately within the same  $\pi$  stack, forming a  $\sim D \sim A \sim D \sim A \sim$   $\pi$ –stacking sequence. Almost all molecular conductors form segregated-stack structures.<sup>1</sup> Although mixed-stack CT complexes do not exhibit metallic electrical conduction, these CT complexes sometimes exhibit peculiar electronic properties such as a neutral (N)–ionic (I) phase transition,<sup>5</sup> quantum dielectric properties,<sup>6</sup> nonlinear conduction,<sup>7</sup> photoinduced phase transitions,<sup>8</sup> and optical switching effects.<sup>9</sup> The first example of an N–I phase transition system was the CT complex made from TTF and chloranil (CA). This system forms a uniform mixed-stack structure and has a neutral electronic ground state of (TTF<sup>+0.3</sup>)(CA<sup>-0.3</sup>) at room temperature, which changes to ionic (TTF<sup>+0.7</sup>)(CA<sup>-0.7</sup>) when the temperature is reduced to 81 K.<sup>5</sup>

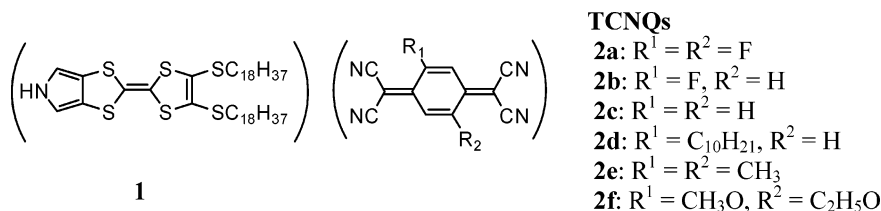
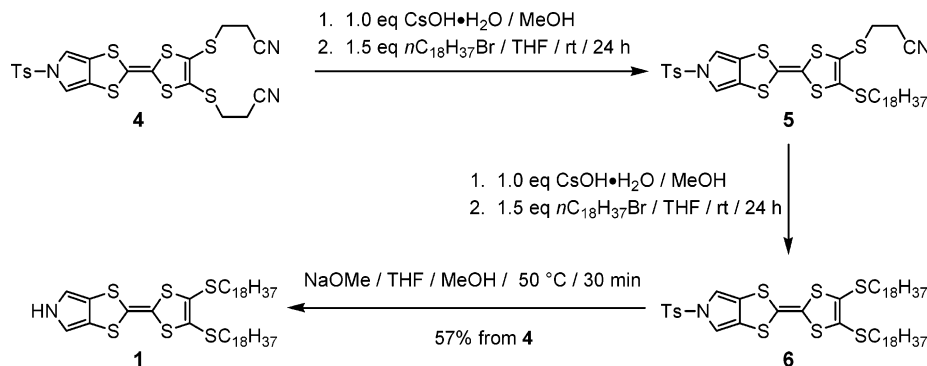
\* To whom correspondence should be addressed. Dr. T. Akutagawa and Prof. T. Nakamura, Research Institute for Electronic Science, Hokkaido University, N12W6 kita-ku, Sapporo 060-0812, Japan. Phone: +81-11-706-2884. Fax: +81-11-706-4972. E-mail: takuta@imd.es.hokudai.ac.jp; tnaka@imd.es.hokudai.ac.jp.

<sup>†</sup> Research Institute for Electronic Science, Hokkaido University.

<sup>‡</sup> CREST, Japan Science and Technology Corporation.

<sup>§</sup> Graduate School of Science, Hokkaido University.

<sup>||</sup> University of Southern Denmark.

SCHEME 1: CT Complexes between the Amphiphilic MP-TTF Derivative **1** and the TCNQ Derivatives **2a–2f**SCHEME 2: Synthesis of the Amphiphilic MP-TTF Derivative **1**

In these mixed-stack structures, competition between  $I_p$ ,  $E_a$ , and electrostatic Madelung energy plays an important role when it comes to the realization of novel physical phenomena.

Electrically active Langmuir–Blodgett (LB) films based on CT complexes have attracted a lot of attention for application in nanoscale molecular devices, such as molecular metals in electrical circuits,<sup>10</sup> rectifiers,<sup>11</sup> nanowires,<sup>12</sup> switches,<sup>13</sup> and sensors.<sup>14</sup> However, to realize these electronic properties within LB films, the electronic structure ( $\delta$ ) and molecular orientation (segregated or mixed stack) of  $(D^{+\delta})(A^{-\delta})$  complexes are important design factors. Although controlling molecular orientation within LB films is quite difficult at present, control of the electronic structure can be achieved by suitable chemical design of the HOMO and LUMO of the D and A, respectively.

In this paper, we describe an efficient method to control the electronic structure of  $(D^{+\delta})(A^{-\delta})$  LB films made from CT complexes between an amphiphilic monopyrrolo-tetrathiafulvalene (MP-TTF, **1**) derivative and different TCNQ derivatives. Pyrrolo-TTFs have in recent years been incorporated into a number of molecular and supramolecular systems, such as sensors, rotaxane-based switches, and devices.<sup>15</sup> Pyrrolo-TTFs have oxidation potentials in an attractive range and have therefore a huge potential for forming CT complexes. This enables a wide range of electron acceptors having different electron affinities to be used. In the present study, six different TCNQ derivatives (**2a–2f**) have been used to control the electronic ground state of LB films (Scheme 1). The electronic ground states of **(1)**(2,5-difluoro-TCNQ) **3a**, **(1)**(fluoro-TCNQ) **3b**, **(1)**(TCNQ) **3c**, **(1)**(decyl-TCNQ) **3d**, **(1)**(2,5-dimethyl-TCNQ) **3e**, and **(1)**(2-methoxy-5-ethoxy-TCNQ) **3f** in LB films were successfully varied from ionic  $(D^{+1})(A^{-1})$  to  $(D^0)(A^0)$  depending on the electron affinity of the TCNQ derivatives.

## Experimental Section

**Synthesis.** Solvents were purchased from Aldrich and purified according to standard procedures. Reagents were purchased from Aldrich except **4** (Scheme 2) which was synthesized according to the literature procedure.<sup>16</sup> Analytical thin-layer chromatography (TLC) was performed on Merck DC-Alufolien Kieselgel 60 F<sub>254</sub> 0.2 mm thickness precoated TLC plates, which were

inspected by UV-light prior to development with iodine vapor. Column chromatography was performed using Merck Kieselgel 60 (0.040–0.063 mm, 230–400 mesh AST0000M). Melting points (mp) were determined on a Büchi melting point apparatus and are uncorrected. High-resolution matrix-assisted laser-desorption/ionization mass spectrometry (HiResMALDI-MS) was performed on an IonSpec Fourier transform mass spectrometer, utilizing a 2,5-dihydroxybenzoic acid matrix. <sup>1</sup>H NMR and <sup>13</sup>C NMR spectra were recorded on a Gemini-300BB (300 and 75 MHz, respectively) spectrometer. All chemical shifts are quoted in ppm on the  $\delta$  scale using TMS or the solvent as the internal standard. Elemental analyses were performed by the Atlantic Microlab, Inc., Atlanta.

**(i) 2-{4-(2-Cyanoethylthio)-5-octadecylthio-1,3-dithiole-2-yliden}-5-tosyl-(1,3)-dithiolo[4,5-c]pyrrole (**5**).** A solution of compound **4** (284 mg, 0.50 mmol) in anhydrous THF (50 mL) was degassed ( $N_2$ , 15 min) before a solution of CsOH·H<sub>2</sub>O (88 mg, 0.53 mmol) in anhydrous MeOH (1.0 mL) was added dropwise via a syringe over a period of 1 h. The mixture was stirred for 15 min, whereupon *n*-octadecyl bromide (250 mg, 0.75 mmol) was added in one portion to the yellow solution. The reaction mixture was stirred for 24 h. After removal of the solvent, the yellow residue was dissolved in CH<sub>2</sub>Cl<sub>2</sub> (100 mL), washed with H<sub>2</sub>O (3 × 50 mL), and dried (MgSO<sub>4</sub>). Concentration gave an orange powder which was purified by column chromatography (silica gel, CH<sub>2</sub>Cl<sub>2</sub>/cyclohexane 2:1,  $R_f = 0.3$ ) to give 324 mg (84%) of **5** as an orange solid: mp 91–92 °C. <sup>1</sup>H NMR (CDCl<sub>3</sub>):  $\delta = 0.88$  (t, 3 H,  $J = 6.4$  Hz), 1.15–1.45 (m, 30 H), 1.62 (quintet, 2 H,  $J = 7.3$  Hz), 2.41 (s, 3H), 2.67 (t, 2 H,  $J = 7.3$  Hz), 2.84 (t, 2 H,  $J = 7.3$  Hz), 3.01 (t, 2 H,  $J = 7.3$  Hz), 6.94 (s, 2 H), 7.30 (d, 2 H,  $J = 8.2$  Hz), 7.73 (d, 2 H,  $J = 8.2$  Hz). <sup>13</sup>C NMR (CDCl<sub>3</sub>):  $\delta = 14.1, 18.6, 21.6, 22.7, 28.5, 29.0, 29.3, 29.5, 29.5, 29.6, 29.6, 29.6, 29.7, 29.7$  (4 signals overlapping), 29.8, 31.3, 31.9, 36.4, 111.3, 111.3, 113.5, 117.5, 118.3, 121.5, 126.9 (2 signals overlapping), 127.0, 130.1, 133.5, 135.3, 145.5. HiResMALDI: Calcd for C<sub>36</sub>H<sub>50</sub>N<sub>2</sub>O<sub>2</sub>S<sub>7</sub>Na ( $M^+ + Na$ ), 789.1809; found, 789.1807.

**(ii) 2-{4,5-Bis(octadecylthio)-1,3-dithiole-2-yliden}-5-tosyl-(1,3)-dithiolo[4,5-c]pyrrole (**6**).** A solution of compound **5** (269 mg, 0.35 mmol) in anhydrous THF (50 mL) was degassed ( $N_2$ ,

15 min) before a solution of CsOH·H<sub>2</sub>O (61 mg, 0.37 mmol) in anhydrous MeOH (1.0 mL) was added dropwise via a syringe over a period of 1 h. The mixture was stirred for 15 min, whereupon *n*-octadecyl bromide (175 mg, 0.53 mmol) was added in one portion to the yellow solution. The reaction mixture was stirred for 24 h. After removal of the solvent, the yellow residue was dissolved in CH<sub>2</sub>Cl<sub>2</sub> (100 mL), washed with H<sub>2</sub>O (3 × 50 mL), and dried (MgSO<sub>4</sub>). Concentration gave an orange powder which was purified by column chromatography (silica gel, CH<sub>2</sub>Cl<sub>2</sub>/cyclohexane 1:3, *R<sub>f</sub>* = 0.3) to give 152 mg (45%) of **6** as a yellow solid: mp 97~98 °C. <sup>1</sup>H NMR (CDCl<sub>3</sub>): δ = 0.88 (t, 6 H, *J* = 6.6 Hz), 1.15~1.45 (m, 60 H), 1.61 (quintet, 4 H, *J* = 7.3 Hz), 2.41 (s, 3H), 2.79 (t, 4 H, *J* = 7.3 Hz), 6.92 (s, 2 H), 7.29 (d, 2 H, *J* = 8.4 Hz), 7.72 (d, 2 H, *J* = 8.4 Hz). <sup>13</sup>C NMR (CDCl<sub>3</sub>): δ = 14.1, 21.6, 22.7, 28.5, 29.1, 29.4, 29.5, 29.6, 29.7 (2 signals overlapping), 29.7 (7 signals overlapping), 31.9, 36.3, 111.2, 115.3, 116.1, 126.9, 127.3, 127.5, 130.1, 135.4, 145.4. HiResMALDI: Calcd for C<sub>51</sub>H<sub>83</sub>NO<sub>2</sub>S<sub>7</sub>, 965.4469; found, 965.4392. Anal. Calcd for C<sub>51</sub>H<sub>83</sub>NO<sub>2</sub>S<sub>7</sub> (966.68): C, 63.37; H, 8.65; N, 1.45; S, 23.22. Found: C, 63.49; H, 8.53; N, 1.44; S, 23.03.

After the desired product **6** was eluted from the column, a second band with *R<sub>f</sub>* = 0.25 containing the detosylated product **1** was isolated. Evaporation of the solvent gave 83 mg (29%) of **1** as a yellow solid.

(iii) 2-{4,5-Bis(octadecylthio)-1,3-dithiole-2-ylidene}-(1,3)-dithiolo[4,5-*c*]pyrrole (**1**). Compound **6** (356 mg, 0.37 mmol) was dissolved in anhydrous THF/MeOH (3:1 v/v, 100 mL) and degassed (N<sub>2</sub>, 15 min) before NaOMe (25% in MeOH, 0.84 mL, 199 mg, 3.68 mmol) was added in one portion. The yellow solution was stirred at 50 °C for 30 min and cooled to room temperature, whereupon most of the solvent was evaporated. The yellow residue was dissolved in CH<sub>2</sub>Cl<sub>2</sub> (100 mL), washed with H<sub>2</sub>O (3 × 50 mL), and dried (MgSO<sub>4</sub>). Concentration gave a yellow oil, which was subjected to column chromatography (silica gel, CH<sub>2</sub>Cl<sub>2</sub>/cyclohexane 1:2, *R<sub>f</sub>* = 0.4) to give 272 mg (91%) of **1** as a yellow solid: mp 92~94 °C. <sup>1</sup>H NMR (CDCl<sub>3</sub>): δ = 0.88 (t, 6 H, *J* = 6.6 Hz), 1.15~1.45 (m, 60 H), 1.60 (quintet, 4 H, *J* = 7.4 Hz), 2.81 (t, 4 H, *J* = 7.4 Hz), 6.60 (d, 2 H, *J* = 2.7 Hz), 8.17 (bs). HiResMALDI: Calcd for C<sub>44</sub>H<sub>77</sub>NS<sub>6</sub>, 811.4380; found, 811.4308. Anal. Calcd for C<sub>44</sub>H<sub>77</sub>NS<sub>6</sub> (812.48): C, 65.04; H, 9.55; N, 1.72; S, 23.68. Found: C, 64.97; H, 9.33; N, 1.78; S, 23.64.

**Electrochemical Measurements.** Redox potentials were obtained using cyclic voltammetry (CV), and the experiments were carried out in anhydrous CH<sub>2</sub>Cl<sub>2</sub> solutions. The working and counter electrode were made of platinum, and a saturated calomel electrode (SCE) was used as the reference electrode. The concentration of the examined compounds was 0.1–0.5 mM, and (*n*-Bu<sub>4</sub>N)(BF<sub>4</sub>) (0.1 M) was added as the supporting electrolyte. The scan rate was 50 mV/s.

**Preparation of CT Complexes and LB Films.** Spectroscopic grade acetonitrile and benzene were used as spreading solvents for preparation of Langmuir monolayers at the air–water interface. TCNQ and 2,5-dimethyl-TCNQ were purchased from Tokyo Kasei Inc. and purified by vacuum sublimation prior to use. Fluoro-TCNQ, 2,5-difluoro-TCNQ, decyl-TCNQ, and 2-methoxy-5-ethoxy-TCNQ were prepared according to the literature procedures.<sup>17</sup> LB films were prepared on aqueous subphases using an NIMA 632D1D2 trough equipped with two moving barriers. The CT complexes **3a–3f** were prepared in situ by mixing equimolar (1.0 mM) quantities of donor **1** and TCNQ derivatives (**2a–2f**) in a 1:1 mixture of CH<sub>3</sub>CN and benzene. These solutions were spread on a milli-Q (>18 MΩ)

water subphase at 291 K. Surface pressure–area ( $\pi$ -*A*) isotherms were recorded at a constant barrier speed of 50 cm<sup>2</sup>/min. Langmuir monolayers of **3a–3f** were transferred onto a freshly cleaved mica surface at a surface pressure of 10 mN/m by a single withdrawal. LB films (20-layer) were transferred onto hydrophobic substrates at a surface pressure of 10 mN/m by horizontal lifting. Quartz and CaF<sub>2</sub> were hydrophobized by deposition of five layers of Cd<sup>2+</sup>–arachidate at a surface pressure of 30 mN/m.

**Atomic Force Microscopy.** AFM images were recorded on a Seiko SPA 400 with an SPI 3800 probe station in tapping mode (dynamic force mode). Commercially available Si cantilevers with a force constant of 20 N/m were used. Surface morphologies of the films transferred onto mica by a single withdrawal were observed as topographic images.

**Optical Spectroscopy.** Polarized UV–vis–NIR (300–3000 nm) and IR (400–7800 cm<sup>-1</sup>) spectra were recorded on a Perkin-Elmer Lambda-19 and a Perkin-Elmer Spectrum 2000 spectrometer, respectively. The 20-layer LB films were transferred onto quartz (20 × 13 mm<sup>2</sup>) for UV–vis–NIR measurements. Polarized UV–vis–NIR spectra were measured using p- and s-polarized light at an angle of incidence of 45° (45p and 45s). Spectra measured using polarized light both parallel and perpendicular to the dipping direction at an angle of incidence of 0° were defined as 90p and 90s, respectively. For IR measurements, transmission (T) and reflection–absorption (RA) spectra of the 20-layer LB films were measured on CaF<sub>2</sub> and evaporated Au substrates, respectively. IR spectra were recorded by 2000 scans of an MCT detector having a resolution of 4 cm<sup>-1</sup>. An angle of incidence of 80° was used for RA measurements.

## Results and Discussion

**Design, Synthesis, and Redox Properties.** The donor molecule **1** (Scheme 1) is composed of a redox active TTF unit, a pyrrole unit, and two hydrophobic *n*-octadecylthio chains. The pyrrole unit is hydrophilic as a consequence of its ability to form hydrogen bonds. The introduction of hydrophobic chains onto the hydrophilic MP-TTF moiety ensures that the molecule **1** is amphiphilic, a criteria which is necessary to form stable Langmuir monolayers of **1** at an air–water interface. The HOMO coefficients of the MP-TTF moiety have been obtained by semiempirical PM3 calculations. These calculations indicate that 13% of the HOMO density of the MP-TTF moiety is located on the pyrrole unit.<sup>16</sup> Therefore, it can be expected that the delocalized  $\pi$  electrons on the MP-TTF moiety can act as the driving force to form stable CT complexes with TCNQ derivatives.

The amphiphilic MP-TTF derivative **1** was synthesized as outlined in Scheme 2. A THF solution of the cyanoethyl protected MP-TTF building block<sup>16b</sup> **4** was treated with 1.0 equiv of CsOH·H<sub>2</sub>O. This procedure generated the TTF-monothiolate, which was alkylated with 1.5 equiv of *n*-octadecyl bromide affording compound **5**. Subsequently, deprotection/alkylation of **5** with 1.0 equiv of CsOH·H<sub>2</sub>O and 1.5 equiv of *n*-octadecyl bromide, respectively, gave (Scheme 2) the TTF derivative **6**. Removal of the tosyl protecting group was carried out by stirring **6** at 50 °C in a 3:1 mixture of THF–MeOH in the presence of an excess of NaOMe, affording the MP-TTF derivative **1** in 57% overall yield from **4**.

The amphiphilic MP-TTF derivative **1** revealed two reversible redox processes at *E*<sub>1/2</sub>(1) = 0.49 and *E*<sub>1/2</sub>(2) = 0.90 V, respectively, which can be associated with the first and second oxidation of **1**. The oxidation potentials for **1** are listed in Table 1, together with the reduction potentials for the TCNQ deriva-

**TABLE 1: Redox Properties of the Amphiphilic MP-TTF Derivative 1 and the TCNQ Derivatives 2a–2f**

	TCNQs	$E_{1/2}(1)$ , V <sup>a</sup>	$E_{1/2}(2)$ , V <sup>a</sup>
<b>2a</b>	2,5-difluoro	+0.50 <sup>b</sup>	-0.14 <sup>b</sup>
<b>2b</b>	2-fluoro	+0.33 <sup>b</sup>	-0.24 <sup>b</sup>
<b>2c</b>	TCNQ	+0.27 <sup>b</sup>	-0.34 <sup>b</sup>
<b>2d</b>	2-decyl	+0.25 <sup>b</sup>	-0.31 <sup>b</sup>
<b>2e</b>	2,5-dimethyl	+0.22 <sup>b</sup>	-0.30 <sup>b</sup>
<b>2f</b>	2-methoxy-5-ethoxy	+0.09 <sup>b</sup>	-0.41 <sup>b</sup>
<b>1</b>		+0.49 <sup>c</sup>	+0.90 <sup>c</sup>

<sup>a</sup> vs SCE in CH<sub>2</sub>Cl<sub>2</sub>, *n*-Bu<sub>4</sub>NBF<sub>4</sub> (0.1 M), Pt working and counter electrodes. <sup>b</sup> Half-wave reduction potentials of TCNQ derivatives. <sup>c</sup> Half-wave oxidation potentials of the MP-TTF derivative 1.

tives **2a–2f**. Typical electron donors, such as TTF, bis(ethylenedioxo)-TTF, and bis(ethylenedithio)-TTF, exhibited under similar conditions  $E_{1/2}(1)$  values at 0.38, 0.45, and 0.56 V, respectively. A comparison of these  $E_{1/2}(1)$  values with the  $E_{1/2}(1)$  value for compound **1** show that the electron donating ability of **1** is higher than that of bis(ethylenedithio)-TTF and is lower than that of TTF. The electron donating ability of donor **1** is comparable to that of bis(ethylenedioxo)-TTF, which previously has been used for the preparation of CT complexes from a variety of acceptors.<sup>18</sup>

Six kinds of TCNQ derivatives (Scheme 1), 2,5-difluoro-TCNQ (**2a**), 2-fluoro-TCNQ (**2b**), TCNQ (**2c**), 2-decyl-TCNQ (**2d**), 2,5-dimethyl-TCNQ (**2e**), and 2-methoxy-5-ethoxy-TCNQ (**2f**), were used to fabricate LB films. Although the redox potentials in solution are affected by the TCNQ solvation energy and radical anion states,<sup>19</sup> the relative magnitude of the electron affinity of these TCNQ derivatives can be predicted from the first reduction potential  $E_{1/2}(1)$ .<sup>20</sup> The  $E_{1/2}(1)$  values of the TCNQ derivatives decreased in the order of **2a** (0.50 V) > **2b** (0.33 V) > **2c** (0.27 V) > **2d** (0.25 V) > **2e** (0.22 V) > **2f** (0.09 V), as shown in Table 1. The variation in electron affinity of compounds **2a–2f** is about 0.4 eV, assuming that the solvation energy for all of the TCNQ derivatives are similar.<sup>20,21</sup> Therefore, the LUMO level of these TCNQ derivatives could vary over a range of 0.4 eV with respect to the HOMO level of the MP-TTF donor **1**.

**Langmuir Monolayers at the Air–Water Interface.** Figure 1 shows the  $\pi$ - $A$  isotherms of Langmuir monolayers of **3a–3f**. Surface pressures of **3a–3f** increase by compression at around  $A_0 = 0.4$  nm<sup>2</sup>, which is close to the cross-sectional area of two closely packed alkyl tails.<sup>22</sup> Because the estimated surface area of donor **1** (~0.7 nm<sup>2</sup>) is much larger than the  $A_0$  values of the CT complexes, the surface area of the floating monolayers of **3a–3f** needs to be determined by the alkyl-chain moieties. The area per molecule at 10 mN/m ( $A_{10}$ ) of monolayers **3a**, **3b**, **3c**, **3d**, **3e**, and **3f** were 0.31, 0.34, 0.29, 0.40, 0.32, and 0.29 nm<sup>2</sup>, respectively. A remarkably sharp increase in the  $\pi$ - $A$  isotherm was observed in the case of **3d**, which can be explained by the presence of an alkyl chain in the acceptor **2d**. A larger  $A_{10}$  value for **3d** than for **3a–3c** and **3e–3f** also suggests that the *n*-decyl chains on **2d** leads to the formation of a more stable molecular-assembly. Because the  $\pi$ - $A$  isotherms of **3a–3f** are fundamentally similar, molecular orientations at the air–water interface are also expected to be similar.

**Surface Morphology of Transferred Films on Mica.** Figure 2 shows the surface morphology of films of **3a**, **3c**, **3d**, and **3e** transferred onto freshly cleaved mica by a single withdrawal. The CT complex covered almost the entire  $10 \times 10 \mu\text{m}^2$  surface area. In higher magnification images ( $2 \times 2 \mu\text{m}^2$ ) of **3a**, **3c**, and **3e** films, domain structures can be observed, whereas a largely uniform surface was obtained for **3d**, reflecting the stability of the floating monolayer at the air–water interface.

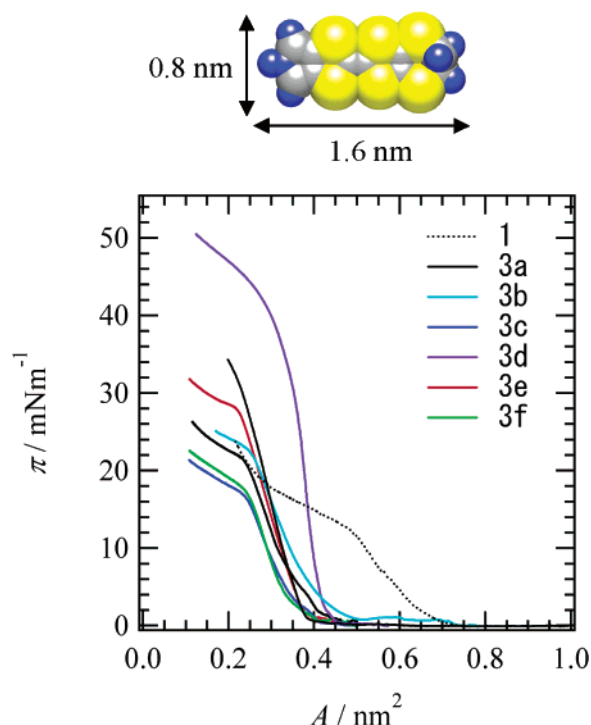


**Figure 1.**  $\pi$ - $A$  isotherms of **1** and **3a–3f** on pure water. The upper part of the figure shows a Cory–Pauling–Koltun (CPK) representation of the MP-TTF derivative **1** viewed normal to its  $\pi$  plane.

Surface morphology of the **3c** film was slightly different as compared to the other films. Higher magnification images reveal a spongelike surface morphology. All of the layers of **3a–3f** on the mica surface have a thickness of ~1.8 nm, which is shorter than the calculated molecular length of octadecane (~2.2 nm),<sup>22</sup> indicating that those layers are monolayers. Interlayer spacing in LB films of orthogonal-packed octadecanoic acid (C<sub>17</sub>H<sub>35</sub>COOH), in which the long axis of the alkyl chains is tilted at ~30° with respect to the substrate normal, has been reported to be ~2.5 nm.<sup>22,23</sup> Therefore, it can be expected that the *n*-octadecylthio chains in the LB films of **3a–3f** on mica surface are tilted, which will be discussed later.

**Electronic State of LB Films.** Table 2 summarizes the CT transition energies ( $h\nu_{CT}$ ) observed in the LB films of **3a–3f** and the difference between the first half-wave oxidation potential of donor **1** and the first half-wave reduction potential of the TCNQ derivatives ( $\Delta E = E_{1/2}(1) - E_{1/2}(\text{TCNQ})$ ). Figure 3 shows electronic absorption spectra of 20-layer LB films of **3a–3f**. The low energy transition at around  $5.3 \sim 6.1 \times 10^3 \text{ cm}^{-1}$  (A band) can be associated with the intermolecular CT transition ( $h\nu_{CT}$ ),<sup>24</sup> whereas the B and C bands are related to the intramolecular excitation of the donor **1** and the TCNQ derivatives, respectively. The solution absorption spectrum of donor **1** recorded in CH<sub>3</sub>CN exhibits the intramolecular  $\pi$ - $\pi^*$  transition at an absorption maximum of  $30.7 \times 10^3 \text{ cm}^{-1}$ , whereas the absorption spectra of CT complexes **3a–3f** recorded in CH<sub>3</sub>CN exhibited intramolecular  $\pi$ - $\pi^*$  transitions at around  $23 \sim 25 \times 10^3 \text{ cm}^{-1}$ . Because the absorption intensities of TCNQ anion radicals in solution are much larger than the absorption intensity of donor **1** in solution, the C bands in the LB films can be expected to originate mainly from the intramolecular excitations of TCNQ anion radicals.<sup>24a</sup> Two characteristic sharp bands at around  $12 \sim 13 \times 10^3 \text{ cm}^{-1}$  were observed in the solution absorption spectra of **3a–3c** and can be associated with

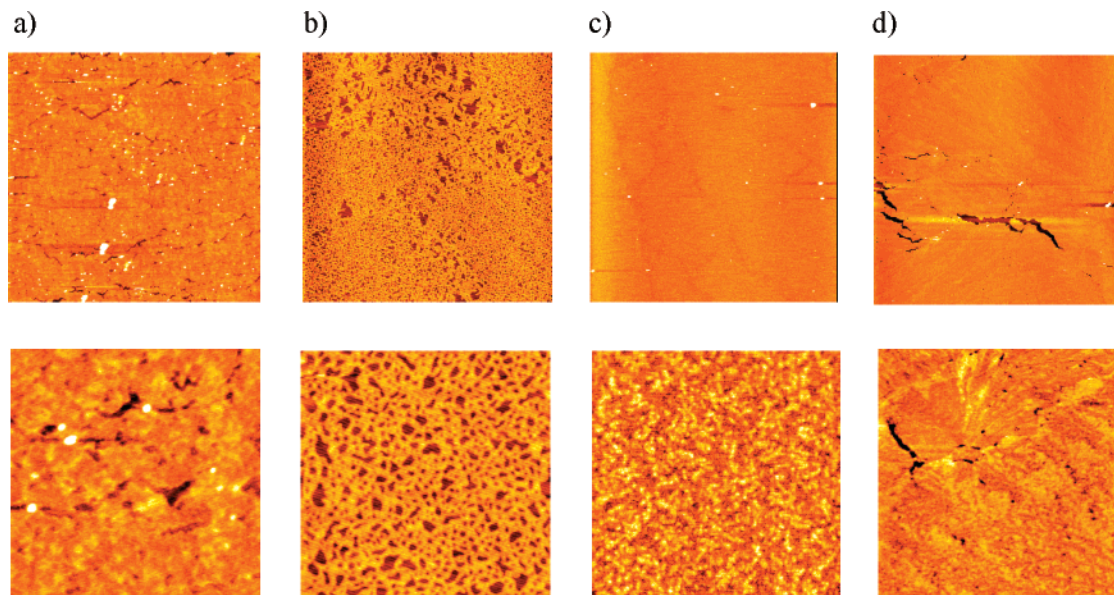


**Figure 2.** Selected AFM images of Langmuir monolayers of (a) **3a**, (b) **3c**, (c) **3d**, and (d) **3e** transferred by a single withdrawal onto a freshly cleaved mica surface ( $\pi = 10$  mN/m). Scales of upper and lower images are  $10 \times 10$  and  $2 \times 2 \mu\text{m}^2$ , respectively.

**TABLE 2: CT Transition Energies ( $h\nu_{\text{CT}}$ ) of LB Films of **3a–3f** and the Difference between the First Half-Wave Oxidation Potential of Donor **1** and the First Half-Wave Reduction Potential of the TCNQ Derivatives ( $\Delta E = E_{1/2}(\mathbf{1}) - E_{1/2}(\text{TCNQ})$ )**

CT complex	$h\nu_{\text{CT}}, 10^3 \text{ cm}^{-1}$	$\Delta E, \text{V}^a$
<b>3a</b>	5.5	-0.01
<b>3b</b>	5.7	+0.16
<b>3c</b>	5.8	+0.22
<b>3d</b>	5.9	+0.24
<b>3e</b>	6.1	+0.27
<b>3f</b>	7.3	+0.40

<sup>a</sup> Difference between the first half-wave oxidation potential of donor **1** and the first half-wave reduction potential of TCNQs.

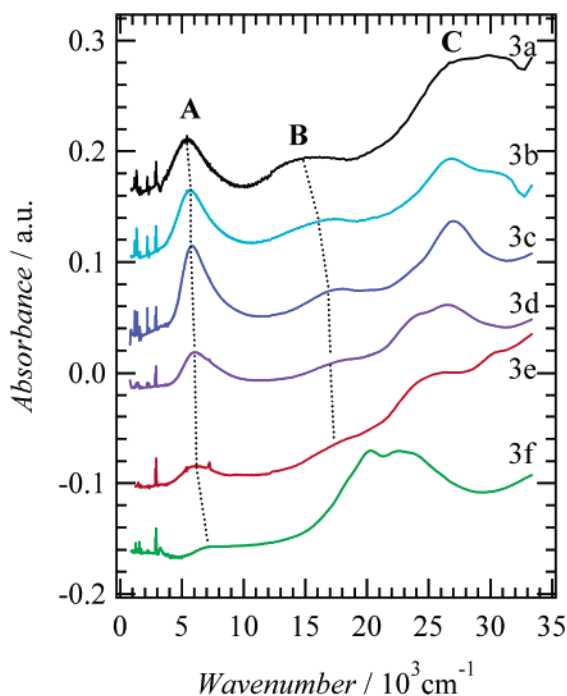


**Figure 3.** UV-vis-NIR-IR spectra of 20-layer LB films of **3a–3f**.

the anion radical species of the TCNQ derivatives.<sup>24a</sup> The absorption intensities of the B bands in the LB films of **3a–3c** were larger than in the other LB films, which can be explained

by a much higher concentration of ionized TCNQ species in the LB films of **3a–3c**. The electronic absorption spectrum of the LB film of **3f** has a different spectral shape as compared to those of **3a–3e**, and an A band at  $7.3 \times 10^3 \text{ cm}^{-1}$  and two broad bands ( $20.2$  and  $22.7 \times 10^3 \text{ cm}^{-1}$ ) were observed. The latter two bands can be assigned to the intramolecular transitions of neutral 2-methoxy-5-ethoxy-TCNQ in the LB film. In solution, these bands were observed at  $22.8$  and  $24.2 \times 10^3 \text{ cm}^{-1}$ , respectively.

The electronic ground state of  $(\text{D}^{+\delta})(\text{A}^{-\delta})$  complexes can be discussed in terms of  $h\nu_{\text{CT}}$  and the difference in redox potentials;  $\Delta E = E_{1/2}(\mathbf{1}) - E_{1/2}(\text{TCNQ})$ , between the electron donor **1** and the electron acceptors (TCNQs) **2a–2f** (Table 2) and can be used to explain the origin of the A bands in electronic absorption spectra.<sup>5,24</sup> Two kinds of methods for predicting the electronic ground state of CT complexes based on  $\Delta E$  have been proposed by Saito et al.<sup>25</sup> and Torrance et al., respectively.<sup>5</sup> In the former case, the partial CT state of  $(\text{D}^{+\delta})(\text{A}^{-\delta})$  with  $0.5 < \delta < 1$ , which is necessary to obtain metallic CT complexes with segregated-stack structures, is achieved under conditions where  $-0.02 < \Delta E < 0.34 \text{ V}$ .<sup>25</sup> Completely ionic  $(\text{D}^{+1})(\text{A}^{-1})$  and neutral  $(\text{D}^0)(\text{A}^0)$  complexes are typically observed under conditions where  $\Delta E < -0.02 \text{ V}$  or  $\Delta E > 0.34 \text{ V}$ , respectively. On the other hand, the latter method can be applied to mixed-stack  $(\text{D}^{+\delta})(\text{A}^{-\delta})$  complexes, in which a phase boundary between ionic  $(\text{D}^{+1})(\text{A}^{-1})$  and neutral  $(\text{D}^0)(\text{A}^0)$  complexes is observed around  $\Delta E = 0.17 \text{ V}$ .<sup>5</sup> Ionic  $(\text{D}^{+1})(\text{A}^{-1})$  and neutral  $(\text{D}^0)(\text{A}^0)$  ground states are typically observed under conditions where  $\Delta E < 0.17 \text{ V}$  or  $\Delta E > 0.17 \text{ V}$ , respectively. The N-I transition of (TTF)(CA) was discovered using this prediction.<sup>5</sup>

If the molecular arrangement of the CT complexes **3a–3f** consists of segregated  $\pi$ -stacked structures of D and A molecules, high electrical conductivity can be expected on account of the presence of mixed valence states and the fact that  $\Delta E$  range from  $-0.01$  to  $+0.40 \text{ V}$  in the CT complexes **3a–3f**. Highly electrically conducting CT complexes also exhibit low energy CT excitations in the IR energy region, which correspond to intra- and inter-band transitions in metal and narrow band-gap semiconductors, respectively.<sup>24</sup> However, the electrical resistivity of the LB films of **3a–3f** was higher than  $100 \text{ M}\Omega\text{cm}$ , with the  $h\nu_{\text{CT}}$  of the LB films observed at energies

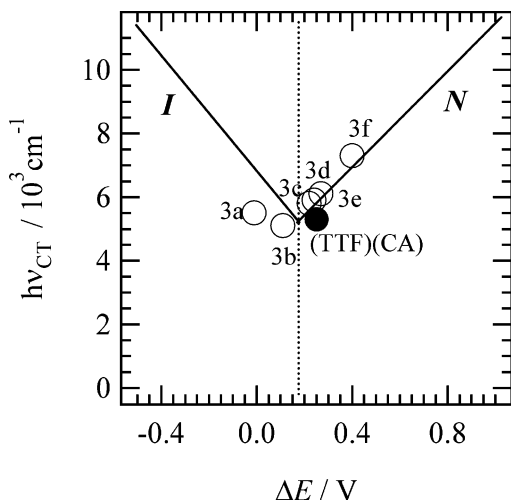


**Figure 4.** Plots of  $h\nu_{CT}$  against  $\Delta E$  for the LB films of **3a–3f** and (TTF)(CA) (closed circle). Equations 1 and 2 are shown as solid lines in the I and N regions, respectively.

above  $5 \times 10^3 \text{ cm}^{-1}$ . Therefore, the  $\pi$ - $\pi$  stacking structures within the LB films of **3a–3f** are mixed stacks rather than segregated stacks. The A bands observed in the electronic absorption spectra of the LB films of **3a–3f** can be accounted for by the presence of intermolecular CT transitions from the HOMO of donor **1** to the LUMO of the TCNQ derivatives.

In cases where the complexes form mixed-stack structures, the boundary conditions of  $\Delta E = 0.17 \text{ V}$  between the ionic and neutral ground states can be applied to predict the electronic structures of the CT complexes. The CT complexes **3a** ( $\Delta E = -0.01 \text{ V}$ ) and **3b** ( $\Delta E = +0.16 \text{ V}$ ) are located in the ionic ( $D^+$ )( $A^-$ ) region, whereas **3c** ( $\Delta E = +0.22 \text{ V}$ ), **3d** ( $\Delta E = +0.24 \text{ V}$ ), **3e** ( $\Delta E = +0.27 \text{ V}$ ), and **3f** ( $\Delta E = +0.40 \text{ V}$ ) are in the neutral ( $D^0$ )( $A^0$ ) region, as shown in Table 2. The CT complexes **3b–3c** are in a  $\Delta E$  region close to the N–I boundary.

The ground state of mixed-stack ( $D^{+\delta}$ )( $A^{-\delta}$ ) complexes can be described by a linear combination of the neutral ( $D^0$ )( $A^0$ ) and the ionic ( $D^+$ )( $A^-$ ) states. The boundary between the ionic and neutral electronic ground states is determined from  $I_p$ ,  $E_a$ , and the electrostatic Madelung energy. Linear  $h\nu_{CT}$  vs ( $I_p - E_a$ ) correlations have been proposed for the ionic and neutral electronic ground states, respectively, according<sup>5</sup> to eqs 1 and 2:

$$h\nu_{CT}(N) = (I_p - E_a) - \left\langle \frac{e^2}{d} \right\rangle \quad (1)$$

$$h\nu_{CT}(I) = -(I_p - E_a) + (2\alpha - 1) \left\langle \frac{e^2}{d} \right\rangle \quad (2)$$

where  $\alpha$  is the Madelung constant and  $d$  is the nearest-neighbor distance between A and D molecules. Equations 1 and 2 meet at  $I_p - E_a = \alpha(e^2/d)$ . When the same solvation energies are applied to the ground and excited-state species, the parameter  $I_p - E_a$  can be replaced by  $\Delta E$ .

Figure 4 shows plots of  $h\nu_{CT}$  against  $\Delta E$  for the LB films of **3a–3f**, together with the theoretical V-shaped line representing eqs 1 and 2. The  $\Delta E - h\nu_{CT}$  plots of **3a** and **3b** appeared at a slightly lower  $h\nu_{CT}$  region than the straight line representing eq 2, whereas those of **3c–3f** are observed to be in agreement with eq 1. The (TTF)(CA) CT complex is located in the neutral region close to the N–I boundary.<sup>5</sup> The  $\Delta E - h\nu_{CT}$  plots of highly conductive segregated-stack CT complexes are typically observed in a much lower  $h\nu_{CT}$  region at around  $2\sim 3 \times 10^3$

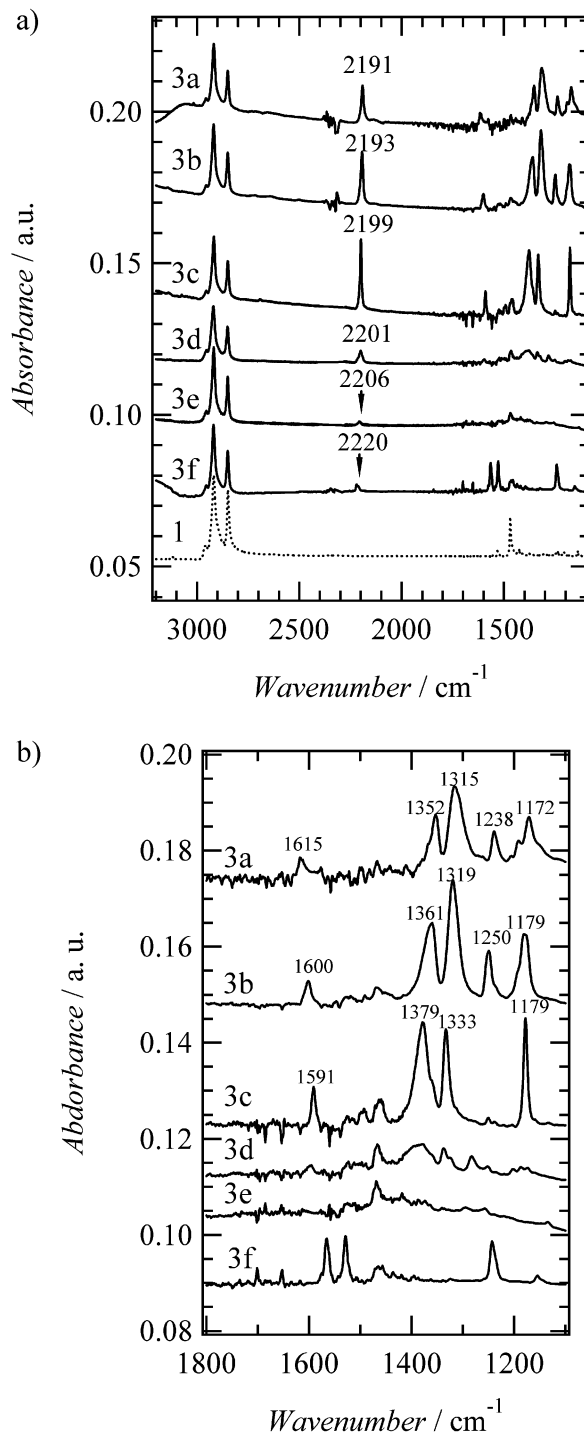


**Figure 5.** Transmission IR spectra recorded of the LB films of **3a–3f** in the frequency ranges of (a) 4000–1400 and (b) 1800–1100  $\text{cm}^{-1}$ .

$\text{cm}^{-1}$ ,<sup>24</sup> in which the CT transition occurs between the same D or A species. The  $\Delta E - h\nu_{CT}$  plots of the LB films of **3a–3f** are consistent with the theoretical predictions for mixed-stack systems, which further support the assignment of the A bands in Figure 3 as intermolecular CT transitions between the HOMO of **1** and the LUMO of the TCNQ derivatives. An inspection of the V-shape diagram reveals that the ionic electronic ground state of ( $D^+$ )( $A^-$ ) is reasonable for the LB films of **3a** and **3b**, whereas the neutral electronic ground state of ( $D^{+\delta}$ )( $A^{-\delta}$ ) for  $\delta < 0.5$  is expected for LB films of **3c–3f**.

**Vibrational Spectra of LB Films.** Several intramolecular vibrational modes are sensitive to the CT state. Figure 5 shows

**TABLE 3: Vibrational Bands Observed in the LB Films of 3a–3f**

LB film	$\nu_{\text{CN}}(a_g)$ , $\text{cm}^{-1}$	$\nu_{\text{CN}}(b_{1u})$ , $\text{cm}^{-1}$	$\nu_3(a_g)$ , $\text{cm}^{-1}$	$\nu_{21}(b_{1u})$ , $\text{cm}^{-1}$	$\nu_5(a_g)$ , $\text{cm}^{-1}$
<b>3a</b>	2191	2203	1615	1352	1172
<b>3b</b>	2193	2207	1600	1361	1179
<b>3c</b>	2199	2210	1591	1379	1179
<b>3d</b>		2212		1393	
<b>3e</b>		2206			
<b>3f</b>		2220			

transmission IR spectra of the LB films of **3a–3f** in the frequency range from 4000 to 1000  $\text{cm}^{-1}$ . In Table 3, typical vibration frequencies observed in the LB films of **3a–3f** are listed. All LB films exhibited two intense vibrational bands at 2918 and 2850  $\text{cm}^{-1}$ , which can be assigned to symmetric and asymmetric  $\nu_{\text{CH}_2}$  modes of the octadecyl chains.<sup>22,23</sup> The IR spectrum recorded of a KBr pellet containing the neutral donor **1** revealed distinctive vibrational modes associated with  $\nu_{\text{CH}_2}$  of the alky chains (2918 and 2849  $\text{cm}^{-1}$ ),  $\nu_{\text{NH}}$  of the pyrrole unit (3400  $\text{cm}^{-1}$ ), and  $\delta_{\text{CH}_2}$  (1470  $\text{cm}^{-1}$ ) of the alkyl chains. The tails of the broad CT transitions are extended to the IR energy region and obscured the  $\nu_{\text{NH}}$  modes in the LB films **3a–3f**. All of the LB films exhibited the nitrile stretching band ( $\nu_{\text{CN}}$ ) expected for TCNQ derivatives at around 2200  $\text{cm}^{-1}$  and some characteristic vibrational bands at frequencies below 1600  $\text{cm}^{-1}$ . The intensity of some of the vibrational bands in the LB films of **3a–3c** is larger than those in the LB films of **3e–3f**, which can be related to different electronic structures and lattice distortions.

Figure 6 shows the transmission (T) and reflection–absorption (RA) spectra recorded of the **3c** LB film. In these two optical arrangements, the transition moment within and normal to the substrate surface is activated in the T and RA spectra, respectively.<sup>22,23</sup> Molecular orientations in the LB films can be determined from the dichroism between the T and RA spectra.<sup>22</sup>

23, 26

Donor **1** contains two hydrophobic octadecyl chains, which have a tendency to assemble with each other through van der Waals interactions in the LB film.<sup>22</sup> The orientation of the octadecyl chains was estimated from the intensity of symmetric ( $\nu_{\text{CH}_2}^s$ ) and asymmetric ( $\nu_{\text{CH}_2}^a$ )  $\text{CH}_2$  stretching modes in the T and RA spectra.<sup>22,23</sup> The enhancement factor  $m$  of the RA spectrum with respect to the T spectrum is given in eq 3:

$$m = 4n_1^3 \sin^2 \theta / n_2^3 \cos \theta \quad (3)$$

where  $n_1$  and  $n_2$  are the refractive indices of air and the film, respectively, and  $\theta$  is the angle of incidence used in RA spectroscopic measurements. A value of  $m = 6.62$  was obtained for the parameters  $n_1 = 1.0$ ,  $n_2 = 1.5$ , and  $\theta = 80^\circ$  in the present measurements.<sup>26d</sup> Because the  $n_2$  values of fatty acid salt LB films have been reported to be around 1.5 from ellipsometry,<sup>27</sup> a value of  $n_2 = 1.5$  was used to obtain the enhancement factor. The average tilt angle  $\phi$  of the uniaxially oriented transition moment from the film normal is given by eq 4:

$$\frac{A_T}{A_R} = \frac{\sin^2 \phi}{2m \cos^2 \phi} \quad (4)$$

where  $A_T$  and  $A_R$  are the absorbance of T and RA spectra, respectively. By applying eq 4 to the  $\nu_{\text{CH}_2}^a$  and  $\nu_{\text{CH}_2}^s$  modes, the tilt angles of symmetric and asymmetric  $\text{CH}_2$  transition moments of  $\phi$  ( $\nu_{\text{CH}_2}^s$ ) and  $\phi$  ( $\nu_{\text{CH}_2}^a$ ) were estimated to be  $70^\circ$  for the **3c** LB film. The tilt angle of the alkyl chains with respect to the

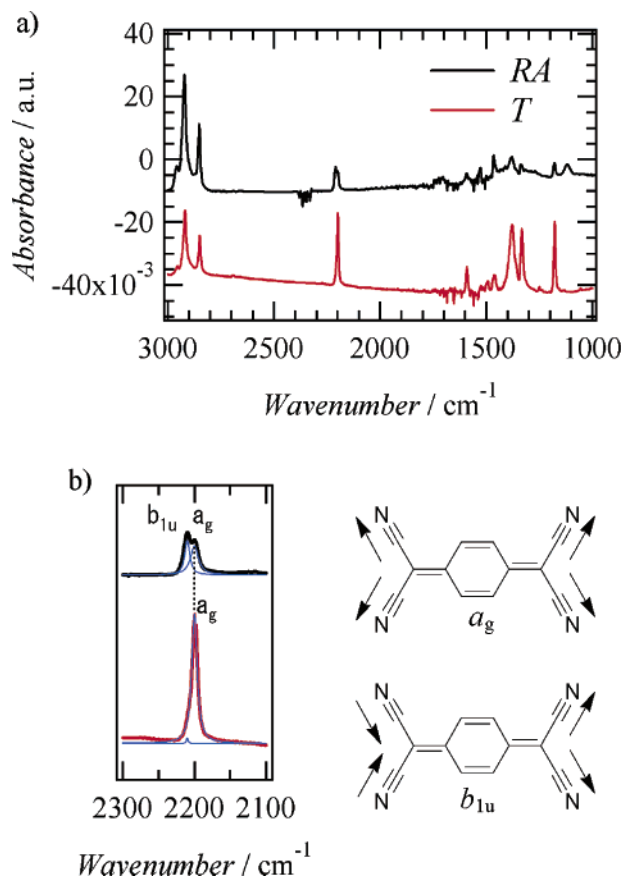


**Figure 6.** Transmission (T) and reflection–absorption (RA) spectra recorded of the **3c** LB film in the frequency ranges of (a) 3000–1000 and (b) 2300–2100  $\text{cm}^{-1}$ . The  $a_g$  and  $b_{1u}$  modes of the  $\nu_{\text{CN}}$  band of TCNQ are also shown. The blue lines in Figure 6b are results of peak deconvolution for  $b_{1u}$  and  $a_g$  modes.

substrate normal ( $\phi_{\text{alkyl}}$ ) was calculated to be  $30^\circ$  by applying the orthogonality relationship  $\cos^2(\phi(\nu_{\text{CH}_2}^s)) + \cos^2(\phi(\nu_{\text{CH}_2}^a)) + \cos^2(\phi_{\text{alkyl}}) = 1$ .<sup>22</sup> Similar tilt angles were observed in LB films of **3a**, **3b**, **3d**, **3e**, and **3f**.

Significant differences between the T and RA spectra in the  $\nu_{\text{CN}}$  band of **3c** LB film were observed, as evidenced in Figure 6b. The  $\nu_{\text{CN}}$  band of TCNQ is composed of three modes having  $b_{1u}$ ,  $b_{2u}$ , and  $a_g$  ( $\nu_2$ ) symmetry.<sup>28</sup> Although the totally symmetric  $a_g$  mode is usually forbidden in IR spectra, lattice distortions such as dimerization within the  $\pi$ -stacking direction activate the  $a_g$  mode in the IR spectra. An intense  $\nu_{\text{CN}}$  band was observed at 2199  $\text{cm}^{-1}$  for the T spectrum of the LB film of **3c**, whereas two  $\nu_{\text{CN}}$  bands at 2210 and 2199  $\text{cm}^{-1}$  were observed in the RA spectrum. The  $\nu_{\text{CN}}(a_g)$  and  $\nu_{\text{CN}}(b_{1u})$  modes of complete ionic ( $\text{K}^+$ )(TCNQ<sup>-1</sup>) appear at 2200 and 2167  $\text{cm}^{-1}$ , respectively.<sup>28</sup> The partially CT ( $N,N$ -dimethylphenazine<sup>+0.5</sup>)(TCNQ<sup>-0.5</sup>) complex exhibited  $\nu_{\text{CN}}(a_g)$  and  $\nu_{\text{CN}}(b_{1u})$  bands at 2198 and 2205  $\text{cm}^{-1}$ , respectively.<sup>29</sup> The energies of the two  $\nu_{\text{CN}}$  bands at 2199 and 2210  $\text{cm}^{-1}$  in the LB film of **3c** were almost consistent with those of ( $N,N$ -dimethylphenazine<sup>+0.5</sup>)(TCNQ<sup>-0.5</sup>) rather than those of ( $\text{K}^+$ )(TCNQ<sup>-1</sup>). Therefore, the electronic ground state of the LB film of **3c** is close to ( $1^{+0.5}$ )(TCNQ<sup>-0.5</sup>), and the  $\nu_{\text{CN}}$  bands at 2199 and 2210  $\text{cm}^{-1}$  can be assigned to  $\nu_{\text{CN}}$  of the  $a_g$  and  $b_{1u}$  modes, respectively. The  $a_g$  symmetry  $\nu_{\text{CN}}$  band was deconvoluted by double Lorentzian (Figure 6b). The  $a_g$  band is activated normal to the TCNQ  $\pi$  plane, and the tilt angle of the transition moment is  $80^\circ$  with respect to the substrate normal accordingly to eq 4. Thus, the TCNQ  $\pi$  plane is tilted at an angle of  $80^\circ$  to the substrate surface, which

corresponds to a largely parallel arrangement of the  $\pi$ -stacking direction to the substrate surface.

Several characteristic vibrational bands were observed (Figure 5b) in the frequency range from 1600 to 1200  $\text{cm}^{-1}$ . Based on the vibrational assignments of (*N,N*-dimethylphenazine<sup>+0.5</sup>)-(TCNQ<sup>-0.5</sup>), the bands at 1591, 1379, and 1179  $\text{cm}^{-1}$  in the **3c** LB film can be assigned to the  $\nu_3$  ( $a_g$ ),  $\nu_{21}$  ( $b_{1u}$ ), and  $\nu_5$  ( $a_g$ ) bands of TCNQ, respectively.<sup>29,30</sup> Among them, the  $\nu_{21}$  band at 1379  $\text{cm}^{-1}$  is useful for determining the parameter  $\delta$  from the linear correlation between neutral TCNQ<sup>0</sup> at 1405  $\text{cm}^{-1}$  to complete ionic TCNQ<sup>-1</sup> at 1361  $\text{cm}^{-1}$ . The  $\nu_{21}$  band of the **3c** LB film was observed at 1379  $\text{cm}^{-1}$ , hence it can be deduced that the **3c** LB film consists of (**1**<sup>+0.6</sup>)(TCNQ<sup>-0.6</sup>). The intensity of the  $a_g$  modes ( $\nu_3$  and  $\nu_5$ ) of **3c** in the T spectrum was larger than those of the RA spectra, which is consistent with the orientation of TCNQ estimated from the  $\nu_{\text{CN}}$  bands.

As the energy of the  $\nu_{21}$  mode of decyl-TCNQ at 1393  $\text{cm}^{-1}$  exhibits the same linear correlation as that of TCNQ, the electronic ground state of the **3d** LB film is estimated to be (**1**<sup>+0.3</sup>)(decyl-TCNQ<sup>-0.3</sup>). The tilt angle  $\phi_{\text{alkyl}} = 30^\circ$  and thickness of the **3d** LB film ( $\sim 1.8$  nm) were similar to those of the **3c** LB film. Although the thickness of the LB films was similar for **3c** and **3d**, the intensity of the vibrational bands of the **3d** LB film was lower than that of the **3c** LB film. The  $a_g$  modes were present in the IR spectra of LB films of **3a–3c**, whereas distinct activation of  $a_g$  modes was not observed in the LB films of **3d–3f**. These results suggest that lattice distortions within the  $\pi$ -stacking axis occurred in the LB films that have an ionic electronic ground state, i.e., the LB films of **3a–3c**. The electronic ground states of the **3c** and **3d** LB films were (**D**<sup>+0.6</sup>)(**A**<sup>-0.6</sup>) and (**D**<sup>+0.3</sup>)(**A**<sup>-0.3</sup>), respectively. Because the vibrational spectra suggest that the **3c** LB film is in the ionic ground state, the N–I phase boundary is expected to be located between the LB film of **3c** and **3d**. The  $\Delta E - h\nu_{\text{CT}}$  plot for the **3d** LB film was close to that of (TTF)(CA),<sup>5</sup> and thus, the possibility of a temperature induced N–I transition was examined. However, the temperature-dependent vibrational spectra of the **3d** LB film does not exhibit any evidence of a N–I transition, even at temperatures below 10 K.

Although complete vibrational assignments of 2,5-difluoro-TCNQ and fluoro-TCNQ have not been reported yet, the vibrational features of the **3a** and **3b** LB films in the frequency range from 1600 to 1200  $\text{cm}^{-1}$  resembled that of the **3c** LB film quite significantly. The  $\nu_{21}$  band of the **3b** LB film was observed at 1361  $\text{cm}^{-1}$ , which is consistent with completely ionic TCNQ<sup>-1</sup> (1361  $\text{cm}^{-1}$ ). On the other hand, the  $\nu_{21}$  band of the **3a** LB film at 1352  $\text{cm}^{-1}$  was located at an intermediate frequency between completely ionic TCNQ<sup>-1</sup> (1361  $\text{cm}^{-1}$ ) and F<sub>4</sub>-TCNQ<sup>-1</sup> (1344  $\text{cm}^{-1}$ ).<sup>28–31</sup> Because the frequency shift of the  $\nu_{21}$  band is dependent on the substituents on TCNQ, an exact determination of the parameter  $\delta$  was impossible for the **3a** and **3b** LB films. However, the results indicate that the electronic ground state of the LB films of **3a** and **3b** are considerably close to the completely ionic (**D**<sup>+1</sup>)(**A**<sup>-1</sup>) state. Because the vibrational spectra of the **3e** and **3f** LB films are superimpositions of neutral **1** and TCNQs, the electronic ground state of these is the neutral (**D**<sup>+ $\delta$</sup> )(**A**<sup>- $\delta$</sup> ) state with  $\delta \sim 0$ .

**Molecular Orientation in LB Films.** Polarized UV–vis–NIR spectra were used to get information about the molecular orientation within the LB films.<sup>22,32</sup> Figure 7a shows the optical arrangement of the measurements, where the dipping direction is nominally abbreviated as *p* for the 90° incidence. All of the LB films of **3a–3f** revealed similar polarization dependence in the UV–vis–NIR energy region. The results for the **3c** LB film

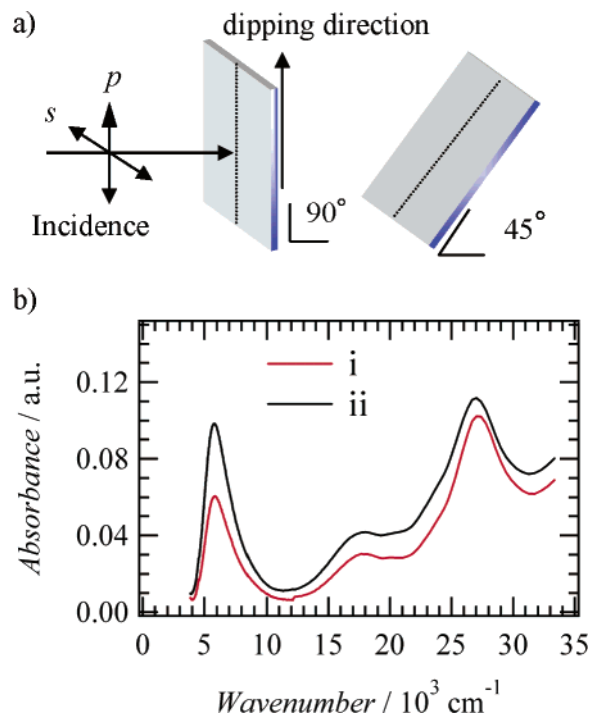


**Figure 7.** Polarized UV–vis–NIR spectra of a LB film. (a) Configuration of the measurements. The dipping direction of the substrate is nominally abbreviated as *p* in normal incidence. (b) UV–vis–NIR spectra recorded of the **3c** LB film for light incident at (i) 45s and (ii) 45p.

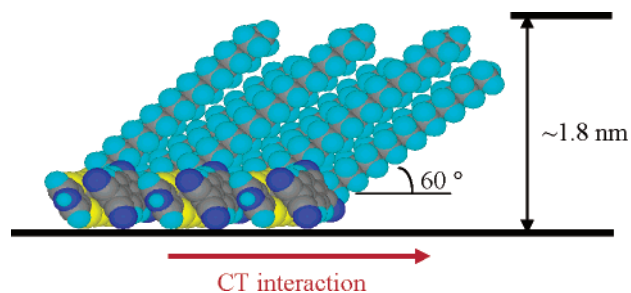


**Figure 8.** Schematic illustration of the molecular orientation of the LB films on a hydrophilic substrate.

are shown in Figure 7b. From the intensities of the spectra with normal incidence of 90p and 90s, the **3c** LB film was estimated to be optically isotropic in the film plane. The intensity of the A band at  $5.8 \times 10^3 \text{ cm}^{-1}$  with *s* polarized light of 45° incidence (spectrum ii) is larger than that of *p* polarized light (spectrum i), which can be accounted for by the largely parallel orientation of the CT transition moment to the substrate surface.<sup>32</sup> The polarization dependence is small for intramolecular transition moments at 17 and  $27 \times 10^3 \text{ cm}^{-1}$ . Because the intramolecular transition moments are along the long axes of TCNQ and donor **1**, the long axes of these molecules are arranged near parallel to the substrate surface. This polarization dependence is consistent with the results obtained from the T and RA IR spectra.

From the polarized IR and UV–vis–NIR spectra and AFM height images, a possible model for molecular packing on the hydrophilic substrate surface was proposed and is shown in Figure 8. The height of a single domain measured by AFM gave a film thickness of  $\sim 1.8$  nm. The octadecyl chains and  $\pi$  plane of TCNQ are tilted at  $\sim 60^\circ$  and  $10^\circ$  with respect to the substrate surface. Considering the direction of CT transitions parallel to the substrate surface, the  $\pi$ -stacking direction between D and

A is expected to occur along the substrate surface. The insulating electrical conductivity and  $h\nu_{CT} - \Delta E$  plot in the V-shape diagram strongly suggest a mixed-stack structure of **1** and TCNQ. Several  $a_g$  modes were activated in the IR spectra of the LB films of **3a–3c**. However, the activation of  $a_g$  modes was not observed in the LB films of **3d–3f**. Because these  $a_g$  modes are principally forbidden in the IR spectra, lattice distortions within the  $\pi$ -stacking axis, such as dimerization, are believed to be present in the LB films of **3a–3c**.

## Summary

CT complexes consisting of an amphiphilic MP-TTF derivative **1** and one of six kinds of TCNQ derivatives were used to fabricate LB films. The electron affinity of the TCNQ derivatives can be varied by more than 0.4 eV by changing the substituents at the 2 and 5 positions of TCNQ from 2-methoxy-5-ethoxy-TCNQ to 2,5-difluoro-TCNQ. Monolayers transferred onto mica surfaces by a single withdrawal were found to be rather uniform, except for the TCNQ complex, which exhibited a spongelike structure. The UV–vis–NIR spectra of these LB films exhibited CT transitions in the NIR–IR energy region, with energies ( $h\nu_{CT}$ ) corresponding to the difference in redox potential ( $\Delta E$ ) between the first oxidation potential of the MP-TTF derivative **1** and the first reduction potential of the TCNQ derivatives. The  $\Delta E - h\nu_{CT}$  plots of the LB films were observed to be in good agreement with the theoretical predictions for mixed-stack CT complexes, an observation which also is consistent with the insulating electrical conductivity of the LB films. From the optical properties, it was deduced that the CT complexes of 2,5-difluoro-TCNQ, fluoro-TCNQ, and TCNQ have ionic electronic ground states, whereas those of decyl-TCNQ, 2,5-dimethyl-TCNQ, and 2-methoxy-5-ethoxy-TCNQ have neutral electronic ground states. Among these LB films, the electronic ground states of (1)(TCNQ) and (1)(decyl-TCNQ) were estimated to be  $(D^{+0.6})(A^{-0.6})$  and  $(D^{+0.3})(A^{-0.3})$ , respectively, which are located around the neutral–ionic phase boundary. The parallel arrangement of the CT transition moment to the substrate surface was confirmed by polarized UV–vis–NIR, transmission IR, and reflection–absorption IR spectra for these LB films. Systematic modulation of the electronic ground state of the CT complexes (1)(TCNQs) is possible by controlling the electron affinity of the TCNQ derivatives, which changes the dipole interaction of the D–A pairs in the thin-film structures. The LB films composed of mixed-stack CT complexes with tunable electronic structures are attractive candidates for the formation of nonlinear optical and dielectric materials.

**Acknowledgment.** This work was partly supported by a Grant-in-Aid for Science Research from the Ministries of Education, Culture, Sports, Science and Technology of Japan and by the Carlsbergfondet in Denmark.

**Supporting Information Available:** The AFM images of the films transferred onto mica surface by a single withdrawal (**3b** and **3f**), transmission and reflection–absorption IR spectra (**3a**, **3b**, **3d**, **3e**, and **3f**), and polarized UV–vis–NIR spectra (**3a**, **3b**, **3d**, **3e**, and **3f**). This material is available free of charge via the Internet at <http://pubs.acs.org>.

## References and Notes

(1) (a) Cowan, D. O. In *New Aspects of Organic Chemistry*; Yoshida, Z., Shiba, T., Oshiro, Y., Eds.; Kodansha: Tokyo, 1989. (b) Saito, G. In *Metal–Insulator Transition Revisited*; Edwards, P. P., Rao, C. N. R., Eds.; Taylor & Francis: London, 1995. (c) *Organic Conductors*; Farges, J.-P., Ed.; Marcel Dekker: New York, 1994. (d) *Handbook of Organic Conductive*

*Molecules and Polymers Vol. 1*; Nalwa, H. S., Ed.; Wiley: Stuttgart, Germany, 1997.

(2) (a) Carlin, R. L. *Magnetochemistry*; Springer-Verlag: New York, 1986. (b) Kahn, O. *Molecular Magnetism*; VCH: Weinheim, Germany, 1992.

(3) (a) *Handbook of Advanced Electronic and Photonic Materials and Devices*; Nalwa, H. S., Ed.; Academic Press: San Diego, CA, 2001. (b) Konuma, T.; Akutagawa, T.; Yumoto, T.; Nakamura, T.; Kawamata, J.; Inoue, K.; Nakamura, T.; Tachibana, H.; Matsumoto, M.; Ikegami, K.; Horiuchi, S.; Yamochi, H.; Saito, G. *Thin Solid Films* **1998**, *327–329*, 348.

(4) (a) Ferraris, J. P.; Cowan, D. O.; Walatka, D. O.; Perlstein, J. H. *J. Am. Chem. Soc.* **1973**, *95*, 948. (b) Khanna, S. K.; Pouget, J. P.; Comes, R.; Garito, A. F.; Hegger, A. *J. Phys. Rev.* **1977**, *16*, 1468. (c) Denoyer, F.; Comes, R.; Garito, A. F.; Hegger, A. *J. Phys. Rev. Lett.* **1975**, *35*, 445. (d) Kagoshima, S.; Anzai, H.; Kajimura, K.; Ishiguro, T. *J. Phys. Soc. Jpn.* **1975**, *39*, 1143.

(5) Torrance, J. B.; Vazquez, J. E.; Mayerle, J. J.; Lee, V. Y. *Phys. Rev. Lett.* **1981**, *26*, 253.

(6) (a) Tokura, Y.; Koshihara, S.; Iwasa, Y.; Okamoto, H.; Komatsu, T.; Koda, T. *Phys. Rev. Lett.* **1989**, *63*, 2405. (b) Horiuchi, S.; Okimoto, Y.; Kumai, R.; Tokura, Y. *Science* **2003**, *299*, 229.

(7) (a) Tokura, Y.; Okamoto, H.; Koda, T.; Mitani, T.; Saito, G. *Phys. Rev. B* **1988**, *38*, 2215. (b) Iwasa, Y.; Koda, T.; Koshihara, S.; Tokura, Y.; Iwasawa, N.; Saito, G. *Phys. Rev. B* **1989**, *39*, 10441. (c) Iwasa, Y.; Koda, T.; Tokura, Y.; Koshihara, S.; Iwasawa, N.; Saito, G. *Appl. Phys. Lett.* **1989**, *55*, 2111.

(8) (a) Koshihara, S.; Tokura, Y.; Mitani, T.; Saito, G.; Koda, T. *Phys. Rev. B* **1990**, *42*, 6853. (b) Koshihara, S.; Takahashi, Y.; Sakai, H.; Tokura, Y.; Luty, T. *J. Phys. Chem. B* **1999**, *103*, 2592.

(9) Iwai, S.; Tanaka, S.; Fujinuma, K.; Kishida, H.; Okamoto, H.; Tokura, Y. *Phys. Rev. Lett.* **2002**, *88*, 57402.

(10) (a) Ikegami, K.; Kuroda, S.; Saito, M.; Saito, K.; Sugi, M.; Nakamura, T.; Matsumoto, M.; Kawabata, Y. *Phys. Rev. B* **1987**, *35*, 3667. (b) Miura, Y. F.; Takenaga, M.; Ksai, A.; Nakamura, T.; Matsumoto, M.; Kawabata, Y. *Jpn. J. Appl. Phys.* **1991**, *30*, 3503. (c) Isotaro, H.; Paloheimo, J.; Miura, Y. F.; Azumi, R.; Matsumoto, M.; Nakamura, T. *Phys. Rev. B* **1995**, *51*, 1809. (d) Nakamura, T. *Handbook of Organic Conductive Molecules and Polymers. Vol. 1 Charge-Transfer Salts, Fullerenes and Photoconductors*; Nalwa, H. S., Ed.; Wiley: Stuttgart, Germany, 1997; p 728. (e) Bryce, M. R.; Petty, M. C. *Nature* **1995**, *374*, 771.

(11) (a) Metzger, R. M.; Chen, B.; HoIpfner, U.; Lakshmintham, M. V.; Vuillaume, D.; Kawai, T.; Wu, X.; Tachibana, H.; Hughes, T. V.; Sakurai, H.; Baldwin, J. W.; Hosch, C.; Cava, O. M. P.; Brehmer, L.; Ashwell, G. *J. Am. Chem. Soc.* **1997**, *119*, 10455. (b) Metzger, R. M. *Acc. Chem. Res.* **1999**, *32*, 950.

(12) (a) Akutagawa, T.; Ohta, T.; Hasegawa, T.; Nakamura, T.; Christensen, C. A.; Becher, J. *Proc. Natl. Acad. Sci. U.S.A.* **2002**, *99*, 5028. (b) Akutagawa, T.; Nakamura, T. In *Semiconductor and Molecular-assembly Nanowires in Chemistry of Nano-molecular Systems – Toward the Realization of Molecular Devices*; Sugiura, K., Matsumoto, T., Tada, H., Nakamura, T., Eds.; Springer-Verlag: Berlin, 2002; p 122.

(13) (a) Tachibana, H.; Nakamura, T.; Matsumoto, M.; Komizu, H.; Manda, E.; Niio, H.; Yabe, A.; Kawabata, Y. *J. Am. Chem. Soc.* **1989**, *111*, 3080. (b) Collier, C. P.; Wong, E. W.; Belohradsky, M.; Raymo, F. M.; Stoddart, J. F.; Kuekes, P. J.; Williams, R. S.; Heath, J. R. *Science* **1999**, *285*, 391. (c) Collier, C. P.; Matternsteig, G.; Wong, E. W.; Lou, Y.; Beverly, K.; Sampaio, J.; Raymo, F. M.; Stoddart, J. F.; Heath, J. R. *Science* **2000**, *289*, 1172. (d) Collier, C. P.; Jeppesen, J. O.; Luo, Y.; Perkins, J.; Wong, E. W.; Heath, J. R.; Stoddart, J. F. *J. Am. Chem. Soc.* **2001**, *123*, 12632. (e) Service, R. F. *Science* **2001**, *294*, 2442. (f) Luo, Y.; Collier, C. P.; Jeppesen, J. O.; Nielsen, K. A.; Delonno, E.; Ho, G.; Perkins, J.; Tseng, H.-R.; Yamamoto, T.; Stoddart, J. F.; Heath, J. R. *ChemPhysChem* **2002**, *3*, 519. (g) Jacoby, M. *Chem. Eng. News* **2002**, *80* (39), 38. (h) Chen, Y.; Ohlberg, D. A. A.; Li, X.; Stewart, D. R.; Williams, R. S.; Jeppesen, J. O.; Nielsen, K. A.; Stoddart, J. F.; Olynick, D. L.; Anderson, E. *Appl. Phys. Lett.* **2003**, *82*, 1610. (i) Chen, Y.; Jung, G.-Y.; Ohlberg, D. A. A.; Li, X.; Stewart, D. R.; Jeppesen, J. O.; Nielsen, K. A.; Stoddart, J. F.; Williams, R. S. *Nanotechnology* **2003**, *14*, 462.

(14) Wohltjen, H.; Barger, E. R.; Snow, A. W.; Jarvis, N. L. *IEEE Trans. Elec. Dev.* **1985**, *ED-32*, 1170.

(15) (a) Jeppesen, J. O.; Perkins, J.; Becher, J.; Stoddart, J. F. *Org. Lett.* **2000**, *2*, 2457. (b) Jeppesen, J. O.; Perkins, J.; Becher, J.; Stoddart, J. F. *Angew. Chem., Int. Ed.* **2001**, *40*, 1216. (c) Nielsen, M. B.; Jeppesen, J. O.; Lau, J.; Lomholt, C.; Damgaard, D.; Jacobsen, J. P.; Becher, J.; Stoddart, J. F. *J. Org. Chem.* **2001**, *66*, 3559. (d) Becher, J.; Brimert, T.; Jeppesen, J. O.; Pedersen, J. Z.; Zubarev, R.; Bjørnholm, T.; Reitzel, N.; Jensen, T. R.; Kjaer, K.; Levillain, E. *Angew. Chem., Int. Ed.* **2001**, *41*, 249. (e) Jeppesen, J. O.; Becher, J.; Stoddart, J. F. *Org. Lett.* **2002**, *4*, 557. (f) Nielsen, K.; Jeppesen, J. O.; Thorup, N.; Becher, J. *Org. Lett.* **2002**, *4*, 1327. (g) Trippé, G.; Levillain, E.; Derf, F. L.; Gorgues, A.; Sallé, M.; Jeppesen, J. O.; Nielsen, K.; Becher, J. *Org. Lett.* **2002**, *4*, 2461. (h) Nielsen, K.; Jeppesen, J. O.; Levillain, E.; Thorup, N.; Becher, J. *Org. Lett.* **2002**, *4*, 4189. (i) Nielsen, K. A.; Jeppesen, J. O.; Levillain, E.; Becher, J. *Angew.*

- Chem., Int. Ed.* **2003**, *42*, 187. (j) Becher, J.; Jeppesen, J. O.; Nielsen, K. *Synth. Met.* **2003**, *133–134*, 309. (k) Li, H.; Jeppesen, J. O.; Levillain, E.; Becher, J. *Chem. Commun.* **2003**, 846.
- (16) (a) Jeppesen, J. O.; Takimiya, K.; Jensen, F.; Becher, J. *Org. Lett.* **1999**, *1*, 1291. (b) Jeppesen, J. O.; Takimiya, K.; Jensen, F.; Brimert, T.; Nielsen, K.; Thorup, N.; Becher, J. *J. Org. Chem.* **2000**, *65*, 5794.
- (17) (a) Anderson, J. R.; Jørgensen, O. *J. Chem. Soc., Perkin Trans. 1* **1979**, 3095. (b) Hasegawa, T.; Inukai, K.; Kagoshima, S.; Sugawara, T.; Mochida, T.; Sugiura, S.; Iwasa, Y. *Chem. Commun.* **1997**, 1377.
- (18) Horiuchi, S.; Yamochi, H.; Saito, G.; Sakaguchi, K.; Kusunoki, M. *J. Am. Chem. Soc.* **1996**, *118*, 8604.
- (19) (a) Grimsrud, E. P.; Caldwell, G.; Chowdhury, S.; Kebarle, P. *J. Am. Chem. Soc.* **1985**, *107*, 4627. (b) Kebarle, P.; Chowdhury, S. *Chem. Rev.* **1987**, *87*, 513. (c) Heinis, T.; Chowdhury, S.; Scott, S. L.; Kebarle, P. *J. Am. Chem. Soc.* **1988**, *88*, 200.
- (20) Chen, E. C. M.; Wentworth, W. E. *Mol. Cryst. Liq. Cryst.* **1989**, *171*, 271.
- (21) Akutagawa, T.; Saito, G. *Bull. Chem. Soc. Jpn.* **1995**, *68*, 1753.
- (22) (a) *Langmuir–Blodgett Films*; Roberts, G., Ed.; Plenum Press: New York, 1990. (b) Ulman, A. *An Introduction to Ultrathin Organic Films*; Academic Press: San Diego, CA, 1991. (c) Petty, M. C. *Langmuir–Blodgett Films; An Introduction*; Cambridge University Press: Cambridge, U.K., 1996.
- (23) Umemura, J.; Kamata, T.; Kawai, T.; Takenaka, T. *J. Phys. Chem.* **1990**, *94*, 62.
- (24) (a) Torrance, J. B.; Mayerle, J. J.; Bechgaard, K. *Phys. Rev. B.* **1979**, *19*, 730. (b) Jacobsen, C. S. In *Optical Properties in Semiconductor and Semimetals. High Conducting Quasi-One-Dimensional Organic Crystals*; Conwell, E., Ed.; Academic Press: New York, 1988.
- (25) Saito, G.; Ferraris, J. P. *Bull. Chem. Soc. Jpn.* **1980**, *53*, 2142.
- (26) (a) Chollet, P.-A.; Messier, J.; Rosilio, C. *J. Chem. Phys.* **1976**, *64*, 1042. (b) Rabolt, J. F.; Burns, F. C.; Schlotter, N. E.; Swalen, J. D. *J. Chem. Phys.* **1983**, *78*, 946. (c) Azumi, R.; Matsumoto, M.; Kuroda, S.; Crossley, M. J. *Langmuir* **1995**, *11*, 4495. (d) Matsumoto, M.; Miyazaki, D.; Tanaka, M.; Azumi, R.; Manda, E.; Kondo, Y.; Yoshino, N.; Tachibana, H. *J. Am. Chem. Soc.* **1998**, *120*, 1479.
- (27) Cresswell, J. P.; Cross, G. H.; Bloor, D.; Feast, W. J.; Petty, M. C. *Thin Solid Films* **1992**, *210–211*, 216.
- (28) (a) Iqbal, Z.; Christoe, C. W.; Dawson, D. K. *J. Chem. Phys.* **1975**, *63*, 4485. (b) Okamoto, H.; Tokura, Y.; Koda, T. *Phys. Rev. B* **1987**, *36*, 3858.
- (29) Meneghetti, M.; Giraldo, A.; Pecile, C. *J. Chem. Phys.* **1985**, *83*, 3134.
- (30) (a) Giraldo, A.; Bozio, R.; Pecile, C.; Torrance, J. B. *Phys. Rev. B* **1982**, *26*, 2306. (b) Painelli, A.; Giraldo, A. *J. Chem. Phys.* **1987**, *87*, 1705.
- (31) Meneghetti, M.; Pecile, C. *J. Phys. Chem.* **1986**, *84*, 4149.
- (32) (a) Matsumoto, M.; Nakamura, T.; Manada, E.; Kawabata, Y.; Ikegami, K.; Kuroda, S.; Sugi, M.; Saito, G. *Thin Solid Films* **1988**, *160*, 61. (b) Ikegami, K.; Kuroda, S.; Tabe, Y.; Saito, K.; Sugi, M.; Matsumoto, M.; Nakamura, T.; Kawabata, Y. *Jpn. J. Appl. Phys.* **1992**, *31*, 1206.